J. Ocean Univ. China (Oceanic and Coastal Sea Research)
https://doi.org/10.1007/s11802-026-6259-y
ISSN 1672-5182, 2026 25 (2): 611-625
http://www.ouc.edu.cn/xbywb/
E-mail:xbywb@ouc.edu.cn

Ammonia Can Damage Hemocytes in *Portunus trituberculatus* by Disrupting MCU-Mediated Mitochondrial Calcium Homeostasis

LIU Yingying[1)], ZHANG Yueqi[2)], CAO Jianwei[2)], ZHAO Chunyan[1)], WANG Wenqi[1)], WANG Fang[2)], CUI Yanting[2), *], and LU Yunliang[1), *]

1) *School of Marine Science and Engineering*, *Qingdao Agricultural University*, *Qingdao* 266109, *China*
2) *Key Laboratory of Mariculture of the Ministry of Education*, *Ocean University of China*, *Qingdao* 266003, *China*

(Received May 2, 2025; revised June 6, 2025; accepted July 21, 2025)

Abstract Calcium (Ca^{2+})-based signaling is vital for responses to environmental stress, with mitochondrial Ca homeostasis being extremely sensitive to changes in cell status. However, the mechanisms by which waterborne ammonia affects mitochondrial Ca dynamics in crustaceans remain unclear. This study examined the impacts of ammonia exposure on mitochondrial Ca^{2+} homeostasis in the hemocytes of the swimming crabs, *Portunus trituberculatus*. Crabs were exposed to varying ammonia concentrations (0, 1, 5, 15, and 45 mg/L) for 24 h and different durations (0, 6, 12, 24, and 48 h) with 15 mg/L ammonia to assess the dose- and time-dependent impacts. Hemocytes were analyzed for Ca^{2+} status and the role of the mitochondrial Ca^{2+} uniporter (MCU) in maintaining it. Ammonia significantly disrupted mitochondrial Ca^{2+} homeostasis, inducing Ca^{2+} overload in the mitochondria and endoplasmic reticulum (ER), reducing cytosolic Ca^{2+} levels, and increasing MCU and sarcoplasmic/ER Ca^{2+}-ATPase (SERCA) expression. These changes were coincident with impaired ATP production, enhanced opening of the mitochondrial permeability transition pore (mPTP), ROS-induced oxidative stress, and loss of membrane potential. MCU inhibition with ruthenium red markedly reduced mitochondrial Ca overload, mPTP opening, autophagic cell fraction, and apoptosis induced by ammonia. These findings suggest that MCU-mediated Ca^{2+} homeostasis is crucial for maintaining mitochondrial function in crustaceans under ammonia-induced stress. The study underscores the importance of understanding environmental adaptive mechanisms in aquatic organisms and proposes potential strategies to mitigate ammonia toxicity by targeting the MCU pathway.

Key words *Portunus trituberculatus*; ammonia; hemocytes; mitochondria; calcium; MCU inhibition

1 Introduction

Excess ammonia-nitrogen (N) in natural or aquaculture ecosystems is a consequence of anthropogenic activities, including wastewater discharge and feeding practices. The detrimental effects of ammonia on aquatic animals, including tissue damage, metabolic suppression, and even reduced growth and survival (Zhao *et al*., 2020; Parvathy *et al*., 2023; Zhang *et al*., 2023), have been extensively documented over the past few decades.

Immune suppression is a typical response to ammonia stress in crustaceans. However, these animals lack an 'adaptive immune system' specific to ammonia and instead rely on the innate immune response against pathogens (Huang and Ren, 2020; Patnaik *et al*., 2024), of which hemocytes are essential regulators. Therefore, maintaining hemocyte homeostasis is vital for the well-being of crustaceans, which can be jeopardized by exposure to high-ammonia environments (HAEs), suppressing the resistance to pathogens (Liu *et al*., 2020; Zhao *et al*., 2020; Li *et al*., 2023a). Substantial hemocyte damage induced by HAEs includes a reduction in the total hemocyte count (THC) and intensification of the apoptotic processes. However, the underlying mechanisms remain ambiguous, with several studies proposing that the accumulation of reactive oxygen species (ROS) and subsequent oxidative stress may be involved (Pinto *et al*., 2016; Liu *et al*., 2020; Li *et al*., 2023b).

ROS accumulation is closely associated with calcium (Ca^{2+}) overload (Antonucci *et al*., 2021; Jomova *et al*., 2023), an intracellular Ca^{2+} status that cannot be maintained normally and therefore results in abnormal cell function (Vassalle and Lin, 2004). Mitochondria serve as a substantial Ca^{2+} reservoir and a pivotal nexus in the Ca^{2+}-based signalling network within cells, attributable to their remarkable capacity for Ca^{2+} influx or efflux (Feissner *et al*., 2009). The mitochondrial Ca^{2+} uniporter (MCU) acts as a highly selective channel, localized in the inner mitochondrial membrane (IMM). It is composed of several structural domains, including coiled-coil transmembrane domains (TMDs). It forms a channel for Ca^{2+} within the MCU complex, in conjunction with the MCU para-

* Corresponding authors. E-mail: yt-cui1114@163.com
E-mail: yun.2004@163.com

log (MCUB), the essential mitochondrial response element, the mitochondrial calcium uptake proteins 1, 2, and 3 (MICU1/2/3), and the MCU regulator 1 (MCUR1) (Nemani *et al*., 2018; Garbincius and Elrod, 2022). Mild Ca^{2+} uptake *via* the MCU can induce transient mitochondrial membrane depolarization and a subsequent enhancement in ROS production by the electron transport chain (ETC) (Feissner *et al*., 2009; Angelova and Abramov, 2024). Conversely, excess Ca^{2+} influx *via* the opening of the mitochondrial permeability transition pore (mPTP) can result in mitochondrial dysfunction and apoptosis. The mPTP comprises multiple proteins located within the mitochondrial membranes and in the matrix (Feissner *et al*., 2009; Orrenius *et al*., 2015; Angelova and Abramov, 2024).

In crustaceans, the mechanism underlying mitochondrial Ca^{2+} homeostasis remains a matter of debate. *In vitro* studies on isolated mitochondria have verified the absence of Ca^{2+}-induced permeability transition in *Artemia franciscana* (Menze *et al*., 2005) and several shrimp species (Holman and Hand, 2009; Konrad *et al*., 2012; Rodriguez-Armenta *et al*., 2021). This phenomenon may be a strategy employed by crustaceans to circumvent apoptosis (Martínez-Cruz *et al*., 2017). Intriguingly, the *in vivo* induction of membrane permeability in the hemocytes of *Penaeus vannamei* infected with WSSV has been demonstrated (Martínez-Cruz *et al*., 2017), yet it has not been replicated *in vitro* using isolated mitochondria (Chen *et al*., 2011). Despite a recent study suggesting MCU-mediated mitochondrial Ca^{2+} uptake in *P. vannamei* (Rodriguez-Armenta *et al*., 2021), the available evidence on MCU-mediated mitochondrial Ca^{2+} homeostasis and its relationship with cell health remains limited and inconclusive. This drawback hampers the advancement of our understanding of the response mechanisms of crustaceans to ammonia.

The swimming crab, *Portunus trituberculatus*, is widely distributed across the north-western Pacific regions and is a commercially vital crustacean species in China. Ammonia exposure induced a decline in THC levels and phagocytic activity in *P. trituberculatus* hemocytes (Yue *et al*., 2010). Our previous work demonstrates that HAEs damage the mitochondria of *P. trituberculatus* hemocytes, accompanied by an increase in ROS levels and causing apoptosis (Lu *et al*., 2025). This finding suggests a close relationship between mitochondrial status and hemocyte health. Considering the key role of the MCU in mitochondrial function, it can be postulated that the dysregulation of MCU-dependent mitochondrial Ca^{2+} homeostasis might exacerbate intracellular ROS-induced stress and the consequent hemocyte apoptosis in *P. trituberculatus*. In this study, crabs were exposed to HAE, and its effects on MCU-mediated mitochondrial Ca^{2+} homeostasis and the associated processes, such as apoptosis, were assessed. To the best of our knowledge, this study represents a pioneering exploration into the mechanism underlying MCU-dependent mitochondrial Ca^{2+} regulation in the hemocytes of crustaceans, and may contribute to an enhanced understanding of the processes by which crustaceans regulate their responses to environmental stress.

2 Materials and Methods

2.1 Crab Husbandry

Swimming crabs were procured from a local farm of the Jiaonan district, Qingdao, Shandong, China. All crabs weighed 115.4 g±22.1 g; n=300, and were sent to the laboratory at the Blue Valley Campus of the Qingdao Agricultural University for an indoor simulation study. Individuals exhibiting no signs of illness or impairment were selected and acclimated for a minimum of two weeks before the commencement of the experiment. During acclimation, the crabs were fed with fresh *Ruditapes philippinarum* clams once daily and cultured in seawater maintained at 23 °C±1 °C and a salinity of about 30, under a photoperiod of 14 h light:10 h darkness. Every day, half of the seawater in each tank was replaced with fresh aerated seawater (pH=7.55–7.85, dissolved oxygen concentration≥6.0 mg/L, and ammonia-N levels<0.2 mg/L).

2.2 Ammonia Exposure and MCU Inhibitor Treatment

Healthy crabs at the intermolt stage were selected for the ammonia exposure experiments. Based on our previous work (Lu *et al*., 2022), ammoniated seawater (total of NH_3 or NH_4^+) was prepared with a 30 g/L NH_4Cl stock solution; ammonia concentration of the fresh seawater was monitored and adjusted every day. For each trial, the crabs were distributed equally among rectangular tanks, 90 cm×60 cm×60 cm. All chosen crabs were deprived of food for 24 h before experiment initiation. The crabs were starved during the ammonia exposure experiments. Crabs in the control group were immersed in natural seawater without any ammonia. Each group consisted of three tanks, each representing one replicate.

Dose-dependent effect of ammonia: The ammonia concentration of the ponds could reach 46 mg/L during cultivation (Chen *et al*., 1988; Yuan *et al*., 2018). Therefore, the ammonia levels in the present study were set at 0–45 mg/L, per our previous study (Lu *et al*., 2022). In this trial, 60 crabs were randomly divided into five groups (12 crabs/group; 4 crabs/tank). Each group was exposed to a specific concentration of ammonia: 0 (control), 1, 5, 15, and 45 mg/L, in a randomized order. Following 24 h of exposure, three from each tank of each group, totaling nine individuals, were randomly sampled.

Temporal impact of ammonia: Healthy crabs were randomly and equally divided into two groups: ammonia exposure and control groups (60 crabs/group; 4 crabs/tank). The ammonia level was 15 mg/L, at which MCU elevated mRNA levels and enhanced protein expression during the dose-effect experiments, accompanied by mitochondrial Ca^{2+} overload. Before experiment initiation (0 h), nine individuals were sampled. Then the crabs were placed into tanks containing ammonia at the specified concentrations. During the experiment, three from each tank of each group, totaling nine crabs, were randomly

chosen for hemolymph sampling at 6, 12, 24, and 48 h.

MCU Inhibitor Treatment: The MCU inhibitor ruthenium red (RR, HY-103311; MedChemExpress LLC., NJ, USA) was employed. Fresh working solutions were prepared in 10 mg/mL in saline. A total of 45 crabs were randomly divided into three groups (15 crabs/group): control (normal seawater+saline injection), ammonia (ammonia exposure+saline injection), and RR (ammonia exposure+RR injection at 2 mg/100 g body weight). RR was injected at doses set according to pre-test results (Fig.S1). An identical volume (220 μL) of all reagents was injected into animals through the ventral sinus *via* the arthrodial membrane at the base of the last pereiopod. The control and ammonia group crabs were immersed in natural seawater without and with 15 mg/L ammonia, respectively. From each group, nine crabs (three from each tank) were randomly sampled, 24 h post-injection.

2.3 Hemolymph Collection and Sample Preparation

At each time interval (dose, temporal, and injection trials), hemolymph (≥8 mL) from each crab was collected from the base of the ventral sinus across the arthrodial membrane. It was then mixed with an anticoagulant solution (8 g/mL sodium citrate, 4.2 g/mL NaCl, and 20.5 g/mL glucose; pH: 7.5) at 1:1 (v:v). Subsequently, the mixture was filtered through a 70-μm nylon membrane to remove cell debris. Next, the mixtures were centrifuged for 15 min at 300×*g* and 4 °C to pellet the cells. The precipitate was resuspended in PBS, and the cell density was adjusted to 1×10^6 cells/mL by quantifying the cells on a TC20™ cell counter (Bio-Rad Laboratories, CA, USA). The suspension obtained was further analyzed.

In the dose trial, the samples of various tissues (the gills, hepatopancreas, muscles, and heart) from the ammonia-stressed crabs were collected at 0 and 24 h to detect the diverse responses in MCU expression.

2.4 RNA-seq

Total RNA from the hemocytes in the ammonia-stressed and control group crabs was extracted and sequenced. To ensure RNA yields sufficient for library preparation, RNA samples from three crabs per tank were mixed, obtaining three pooled samples for each group. After assessing RNA quality, the cDNA libraries were constructed and sequenced on a NovaSeq 6000 platform (Illumina, CA, USA). After filtering the raw sequences, clean reads were obtained and aligned to the reference genome. The fragment per kilobase of transcript per million mapped reads (FPKM) was calculated to identify the differentially expressed genes (DEGs), which are defined as those with a false discovery rate (*FDR*)<0.05 and absolute fold change≥2. Gene Ontology (GO) and pathway enrichment analyses were then conducted. The detailed method is available in the supplementary File S1.

2.5 Transmission Electron Microscopy (TEM)

Following a 24-h exposure to 15 mg/L ammonia during the dose trial, 1×10^6 hemocytes were collected from the control and treatment group crabs; one from each tank was randomly selected. After centrifugation for 8 min at 500×*g* and room temperature, the pellets were fixed with 3% glutaraldehyde solution (G5882; Sigma-Aldrich, MO, USA) for 24 h at 4 °C. Subsequently, they were subjected to a series of ethanol dehydration steps, and then embedded in Epon812 epoxy resin (Sigma-Aldrich). Following incubation at 37, 45, or 65 °C for 24 h, cured samples were collected, and ultrathin sections were obtained with an EM UC6 Ultracut microtome (Leica Microsystems, Wetzlar, Germany). Subcellular structural changes were observed with a JEM-1200EX TEM (JEOL, MA, USA) after uranyl acetate+lead nitrate staining.

2.6 MCU Bioinformatics

The MCU protein sequence (394 amino acids) was obtained from NCBI (https://www.ncbi.nlm.nih.gov/; Accession no. XP_045122017). The MCU three-dimensional structure was predicted using the SWISS-MODEL server (https://swissmodel.expasy.org/), and the structure with the highest similarity to that of the query sequence was selected as the potentially appropriate model. The amino acid sequences from vertebrate and invertebrate homologs (Table 1) were comprehensively aligned utilizing the DNAMAN software (https://www.lynnon.com/dnaman.html) with the following parameters: full alignment, gap penalty set at 3, and k-tuple set at 1, while retaining≤5 top diagonals for efficient sequence comparison. The phylogenetic tree was constructed based on the coding region sequences (CDS) of the MCUs from various species, by employing the Neighbor-Joining method with 1000 bootstrap replicates and using the MEGA6 software (https://www.megasoftware.net/).

Table 1 Accession numbers of the MCU homologs identified in various species

Species name	Accession no.
Procambarus clarkii	XP_069181617.1
Homarus americanus	XP_042239133.1
Penaeus chinensis	XP_047477134.1
Portunus trituberculatus	XP_045122017.1
Drosophila melanogaster	NP_001246647.1
Homo sapiens	NP_001257608.1
Oreochromis niloticus	XP_025753054.1
Danio rerio	NP_001070793.1
Mus musculus	NP_001028431.2
Macaca mulatta	XP_015002890.1
Penaeus monodon	XP_037786946.1
Cherax quadricarinatus	XP_053629050.1
Laodelphax striatellus	RZF40471.1
Periplaneta americana	KAJ4445573.1
Helicoverpa armigera	XP_021185393.1
Colias croceus	XP_045498778.1
Felis catus	XP_023096312.1

2.7 qRT-PCR

The total RNA was extracted from each hemocyte sample with the TransZol Up RNA Kit (ER501, TransGen

Biotech) according to the manufacturer's instructions. After confirming the RNA quality and quantity on a NanoDrop 2000 (Thermo Scientific), it was reverse transcribed into cDNA with the Evo M-MLV Reverse Transcription Kit (11705; Accurate Biology (AcciBio), Guangzhou, China).

The gene expression profile was determined using the CFX96Touch™ qPCR System and the SYBR® Green dye (Bio-Rad, USA). The sequences of the primers used are presented in Table 2. The reaction mix (20 μL) was composed of 10 μL of 2× SYBR® Green Pro Taq HS Premix II, 2 μL of diluted cDNA, 0.8 μL each of the forward and reverse primers, and 7.2 μL of DNase-free water. The PCR program comprised an initial activation step at 95 °C for 30 min, followed by 95 °C for 5 s (40 cycles) and 60 °C for 30 s. The relative gene expression levels were calculated per the $2^{-\Delta\Delta CT}$ method with *β-actin* as the internal control.

Table 2 Sequences of the primers used to amplify the target and reference genes

Gene	Primer	Primer sequence (5'–3')	Accession no.	Gene function
β-actin	F	AGCGAGGCTACACCTTCAC	XP_045117304.1	Housekeeping gene
	R	TCCAGGGAGGAGGAAGAAG		
MCU	F	ACCACTCAGGCAGAACACT	XP_045122017.1	Calcium channel in the inner mitochondrial membrane (Garbincius and Elrod, 2022; Matuz-Mares *et al*., 2022)
	R	CCCTCAACCTACCTCACTC		
Leucine-zipper and EF-hand-containing TransMembrane protein 1 (*LETM1*)	F	AGTCTGCCAACTCGCTCTT	XP_045129947.1	Ca^{2+}/H^{+} antiporter in the inner mitochondrial membrane (Garbincius and Elrod, 2022; Matuz-Mares *et al*., 2022)
	R	CATTTATCCCAGCCACTCC		
Sarcoplasmic/ER Ca^{2+} ATPase (*SERCA*)	F	AGGTTGGGCTCACAGACGC	XP_045110898.1	Pumps Ca^{2+} into the ER/SR (Luciani *et al*., 2009; Loncke *et al*., 2020)
	R	CTCTTGGAACGGACTGGAC		
Inositol trisphosphate receptor (*IPR*)	F	CCTACTCGCACCTTCTCAC	XP_045113402.1	Release Ca^{2+} from the ER (Luciani *et al*., 2009; Loncke *et al*., 2020)
	R	CTACGGCAATGCTGTTCTC		
Phosphoinositide-specific phospholipase C (*PLC*)	F	ATAGTTCGTTCACAGCCAC	XP_045101169.1	Endoplasmic reticulum Ca^{2+} channels open and release Ca^{2+} into the cytoplasm (Stefan, 2020)
	R	GAAAGGCAGAAGTGCTAAA		
Plasma membrane Ca^{2+} ATPase (*PMCA*)	F	CAGGGTTCCAGTCTTGTCT	XP_045133482.1	Transport Ca^{2+} from the cytosol to the external environment (Bruce, 2018)
	R	TGCCTTCATTATTGCTGTC		

2.8 Quantification of MCU Expression by ELISA

The MCU ELISA Kit (Omnimabs, CA, USA) was utilized to quantify the expression of the MCU protein. In a microtiter plate well, 10 and 40 μL of the sample and diluent, respectively, were mixed. After adding 100 μL of the HRP-conjugate reagent, the mixture was incubated at 37 °C for 60 min. Each well was then washed five times with the wash solution provided in the kit. The final reaction system was added with 50 μL each of the chromogen solutions A and B and dark-incubated at 37 °C for 15 min. Finally, 50 μL of the stop solution was added, and the OD_{450} was read on a Synergy™ multifunctional enzyme plate analyzer (BioTek, Agilent Technologies Inc., CA, USA). The protein concentration (mg/mL) was calculated using a standard curve.

2.9 Flow Cytometry

Mitochondrial membrane potential (ΔΨm): 5,5',6,6'-tetraethylbenzimidazolocarbocyanine iodide (JC-1) exists in a monomer state at a lower ΔΨm, whereas it forms polymers (J-aggregates) at a higher ΔΨm, within the mitochondrial matrix. Estimating the change in ΔΨm by measuring the green (monomer) and red (aggregate) fluorescence signal intensities constitutes a reliable method. Following the protocol of the ΔΨm assay kit (Beyotime Biotechnology, Shanghai, China), the hemocyte suspension was combined with the JC-1 working solution in a ratio of 1:1, and dark-incubated at 37 °C for 20 min. Following this, the mix was centrifuged at 600×*g* and 4 °C for 4 min. The pellet was then washed twice with the staining buffer (1×) and resuspended in it. The fluorescence of the final solution was measured at excitation/emission wavelengths ($\lambda_{ex}/\lambda_{em}$=Ex/Em) of 525 nm/590 nm with a CytoFLEX S flow cytometer (Beckman Coulter, Inc., CA, USA).

mPTP opening: The opening of the mPTP was identified using a fluorescent probe, calcein AM (Ex/Em: 494 nm/517 nm), and an mPTP assay kit (Beyotime Biotechnology). In brief, 1000 μL of a hemocyte suspension was loaded with 100 μL of calcein AM and dark-incubated at 37 °C. Then the mixture was centrifuged at 1000×*g* and room temperature for 5 min. The pellet was washed with PBS and resuspended in 400 μL of the 1× assay buffer for flow cytometry.

Intracellular Ca^{2+} levels: The Ca^{2+} flux in the hemocytes was analyzed, by employing the fluorescent probes Fluo-4 AM (Ex/Em: 490 nm/525 nm; AAT Bioquest, CA, USA), Rhod-2 AM (Ex/Em: 540 nm/590 nm; AAT Bioquest), and Mag-Fluo-4 AM (Ex/Em: 494 nm/516 nm; AAT Bioquest) to measure the Ca^{2+} concentrations in the cytoplasm, mitochondria, and endoplasmic reticulum (ER), respectively. The procedures for using these three dyes were analogous and followed the manufacturer's protocols. In summary, the appropriate working solution

(1×) was added to a cell plate containing the suspension. The dye-loaded plate was then dark-incubated at 37 °C for 60 min. Thereafter, the working solution was replaced with HHBS to remove the excess probes. The fluorescence intensity of the final solution was quantified with a flow cytometer.

Intracellular ROS levels: The intracellular ROS levels of the hemocytes in the injected crabs were detected by using 2',7'-dichlorodihydrofluorescein diacetate (H2D CFDA; HY-D0940; Ex/Em: 488 nm/525 nm; MedChemExpress). For the assay, 40 μL of the freshly prepared H2DCFDA working solution was added to 400 μL of the hemocyte suspension. The mixture was dark-incubated at room temperature for 30 min, then centrifuged at 600×*g* for 5 min. The pellet obtained was resuspended in PBS, and the fluorescence intensity was detected on a flow cytometer.

Hemocyte autophagy: The Cyto-ID® Autophagy Detection Kit (ENZ-51031-K200; ENZO Life Sciences, NY, USA) was utilized to quantify the autophagy flux in the hemocytes of the injected crabs by labeling the phagophores, autophagosomes, and autolysosomes. Per the manufacturer's instructions, 400 μL each of the hemocyte suspension and the Cyto-ID® working solution were mixed and dark-incubated at room temperature for 60 min. Subsequently, the mixture was centrifuged at 600×*g* and room temperature for 5 min. The precipitate obtained was washed with PBS and resuspended in 400 μL of the 1× assay buffer. The fluorescence intensity was determined on a flow cytometer (Beckman Coulter), which was equipped with an FITC channel. Using flow cytometry, the negative and positive cells that were unlabeled or labeled with Cyto-ID® were distinguished. The ratio of cells labeled with Cyto-ID® to the total number of cells was employed to reflect the change in autophagy.

Measurement of apoptosis: The Annexin V-FITC Apoptosis Detection Kit (CA1020; Solarbio, Beijing, China) was utilized to analyze apoptosis of the hemocytes from injected crabs. A mixture containing 400 μL of the hemocyte suspension and 5 μL of the Annexin V-FITC solution was dark-incubated at room temperature for 5 min. After adding 5 μL of the PI solution and 400 μL of PBS, a flow cytometry was conducted at a λ_{ex} of 488 nm. Apoptosis was defined based on the percentage of hemocytes exhibiting apoptotic characteristics, including cells in the early and late apoptotic states (Annexin V-FITC or Annexin V-FITC+PI positive, respectively).

2.10 ATP Contents

The ATP content of the hemocytes from ammonia-stressed crabs was determined with an ATP assay kit (Beyotime Biotechnology). For each sample, 200 μL of lysis buffer was added to 500 μL of the hemocyte suspension. After incubation for 10 min, the mixture was centrifuged at 4 °C and 12000×*g* for 5 min. Of the supernatant, 20 μL was mixed with 100 μL of the working solution. The luminescence intensity was then measured with a spectrophotometer (BioTek Instruments, Inc., VT, USA). A standard curve for ATP was plotted to calculate the ATP levels in each sample.

2.11 Statistical Analysis

The data were normalized to the control group and expressed as the means±S.D. Statistical analysis of the data used the SPSS 22.0 software (IBM, NY, USA). Pearson correlation was employed to analyze the relationship between the changes in MCU and Ca^{2+} homeostasis and those in ROS, autophagic cell fraction (ACF), and apoptosis, which were assessed in our previous study. The Kolmogorov-Smirnov and Levene's tests were used to ascertain the normality and homogeneity of variances, respectively. Then, an independent sample *t*-test or one-way ANOVA followed by Tukey multiple comparisons test was performed, with $P<0.05$ indicating statistical significance.

3 Results

3.1 MCU Is Involved in Ammonia-Induced Mitochondrial Damage

Figure 1 illustrates the impact of ammonia exposure on the hemocytes at the transcriptome level. RNA-seq analysis identified 226 downregulated and 138 upregulated DEGs (Fig.1B). These gene expression profiles indicated that more number of genes were downregulated post-ammonia exposure (Figs.1C and D). Primarily, GO terms belonging to biological process, cellular component, and molecular function were downregulated in the treatment group (Fig.1G). The TEM images revealed conspicuous damage to the hemocytes, including nuclear condensation and mitochondrial swelling or vacuolization (Fig.1E). The enriched mitochondria-related DEGs also indicated a compromised mitochondrial state, as the expression of most genes was suppressed (Fig.1F). However, the MCU activity was enhanced. Consequently, it can be postulated that ammonia may damage hemocytes by affecting MCU-mediated mitochondrial Ca^{2+} homeostasis.

3.2 Bioinformatic Analysis of MCU and Tissue-Specific mRNA Expression

As the function of ptMCU has not been documented, we initially analyzed the available bioinformatic data (Fig.2). The predicted tertiary structure of the ptMCU was mainly composed of α-helices, with a few random coils and β-sheets (Fig.2A).

The multiple sequence alignment and phylogenetic tree analysis results demonstrated that this protein exhibits high levels of interspecies conservation, including *Homo sapiens*, *Drosophila melanogaster*, *Danio rerio*, and *P. trituberculatus*. However, it exhibited distinct characteristics when compared to those of others, such as *Cherax quadricarinatus* (Figs.2B and C). Additionally, *ptMCU* exhibited tissue-specific expression patterns post-ammonia exposure (Fig.2D), with the maximum upregulation observed in the hemocytes.

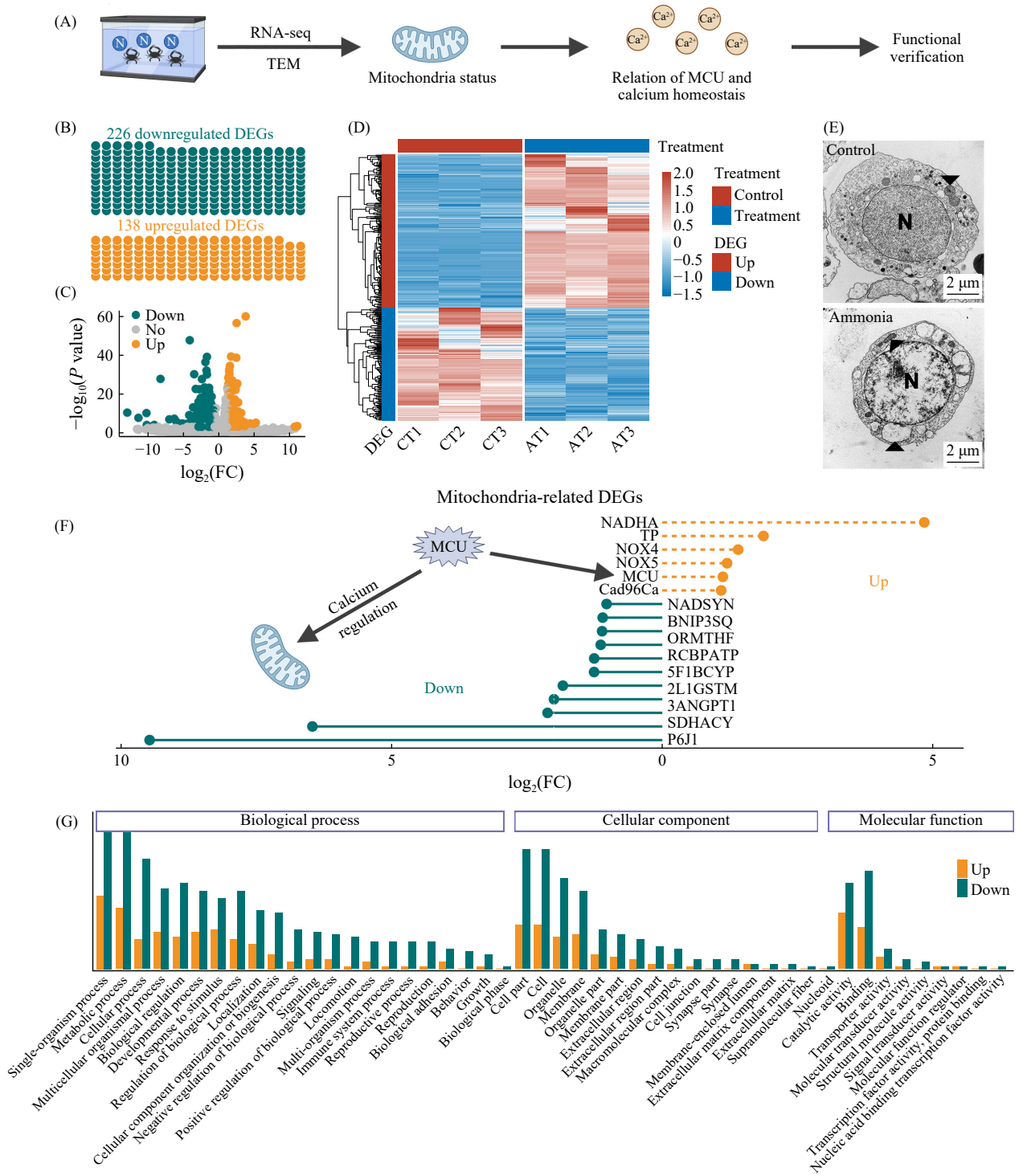

Fig.1 Analysis of hemocyte mitochondrial status using RNA-seq and transmission electron microscopy (TEM). (A) Workflow of the present study. After 24 h of ammonia exposure, the hemocytes were collected for RNA-seq and TEM imaging. (B) Waffle chart indicates the differentially expressed genes (DEGs). (C) Volcano map of the DEGs. (D) Heatmap of the DEGs. (E) TEM images displaying the subcellular structures of hemocytes. (F) Mitochondria-function-related DEGs that were detected. The dysregulation of genes such as *MCU* indicates impaired mitochondrial functioning. (G) GO analysis of the DEGs.

3.3 Dose and Temporal Effects of Ammonia on Hemocyte Calcium Levels

Following exposure to varying concentrations of ammonia, a notable alteration in the hemocyte Ca^{2+} levels was detected. Notably, ammonia exposure reduced the cytoplasmic Ca^{2+} ($[Ca^{2+}]_C$) levels (F [4, 30]=968.633, P=0; Fig.3B). Conversely, the total Ca^{2+} levels were elevated in the cell: $[Ca^{2+}]_t$, ER: $[Ca^{2+}]_{ER}$, and mitochondria: $[Ca^{2+}]_m$ (F [4, 30]=48.824, 315.579, and 194.874, respectively, P=0; Figs.3A, C, D]. The $[Ca^{2+}]_m$ exhibited distinct fluctuations compared to $[Ca^{2+}]_{ER}$, with the former peaking at 5 mg/L ammonia, while the latter exhibited an incremen-

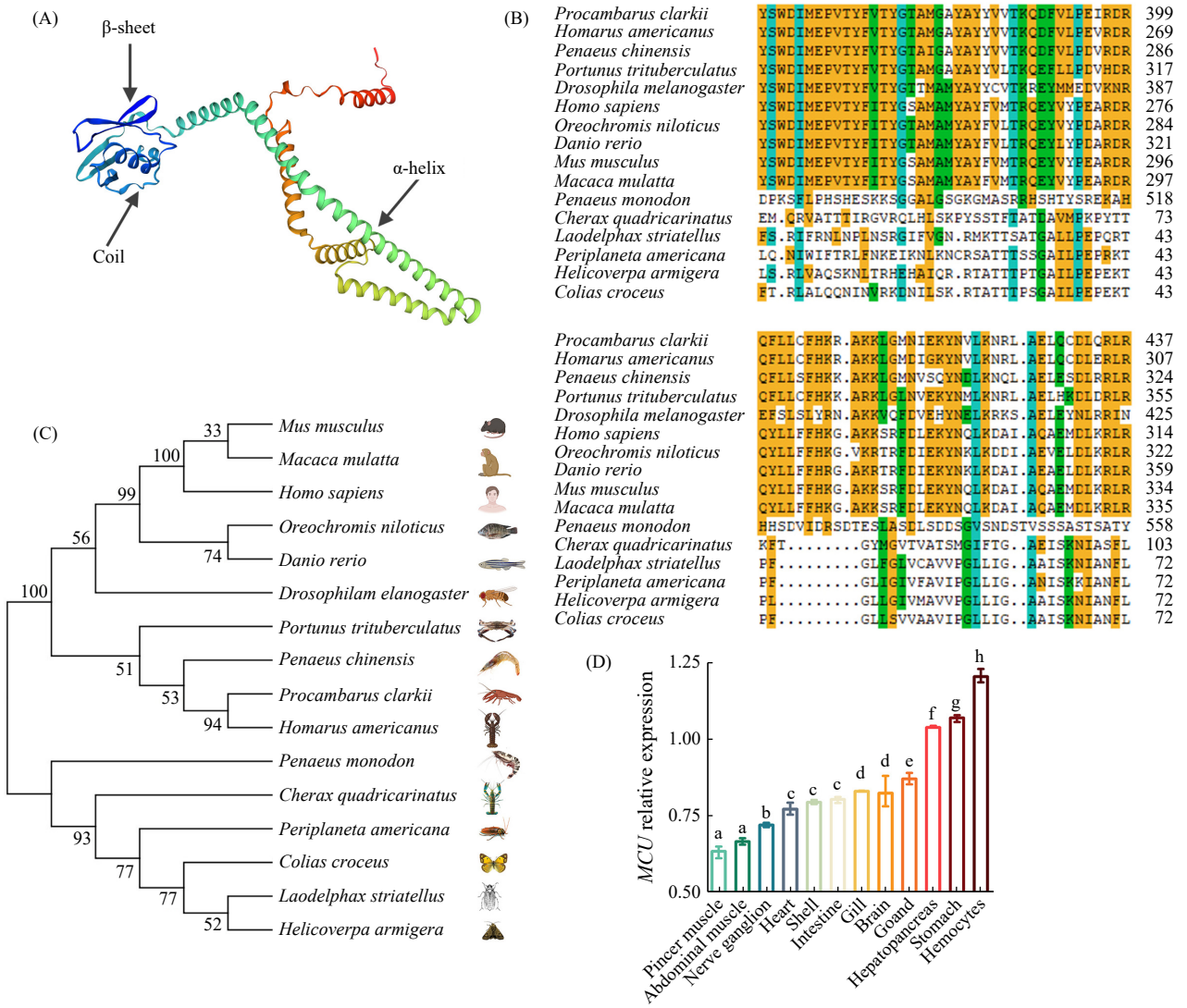

Fig.2 Structure prediction, homology analysis, and tissue-specific expression of MCU in *P. trituberculatus*. (A), prediction of the ptMCU structure using SWISS-MODEL; (B), multiple sequence alignment of the MCUs from vertebrate and invertebrate species; (C), a phylogenetic tree constructed using MEGA6; (D), ammonia-induced fold changes in *ptMCU* mRNA expression (relative to the levels before ammonia exposure) in different crab tissues. The lowercase letters above the columns indicate significant differences in the ammonia-induced fold change in *ptMCU* expression between tissues calculated *via* ANOVA and multiple comparisons.

tal increase with ammonia dose (Figs.3C and D). Ammonia exposure increased mPTP opening in the mitochondria (F [4, 30]=76.954, P=0; Fig.3E), reaching a maximum at 15 mg/L ammonia. However, the ΔΨm was elevated at <5 mg/L ammonia yet suppressed at 15 and 45 mg/L (F [4, 30]=450.462, P=0; Fig.3F).

A discernible alteration in the hemocyte Ca^{2+} homeostasis was observed in response to ammonia exposure (Fig.4). As the concentration of ammonia rose, the $[Ca^{2+}]_t$ elevated (F [4, 30]=44.512, P=0; Fig.4A), but the $[Ca^{2+}]_C$ declined (F [4, 30]=270.473, P=0; Fig.4B). The $[Ca^{2+}]_{ER}$ and $[Ca^{2+}]_m$ were also elevated by ammonia but exhibited an initial increase followed by a decrease, reaching their highest levels at 6 to 12 h (F [4, 30]=68.878 and 255.006, P=0; Figs.4C, D). Maximal mPTP opening and ΔΨm loss occurred within 12 h of ammonia exposure (F [4, 30]=57.643 and 52.199, P=0; Figs.4E, F). After 24 h of exposure, the ΔΨm, however, returned to a level below that of the control (Fig.4F).

3.4 Dose and Temporal Effects of Ammonia on Ca^{2+}-Related Genes

Ammonia-induced stress significantly reduced the mRNA levels of *LETM* and *IPR* (F [4, 30]=301.370 and 224.549, P=0). The *LETM* expression levels reached their minimum at 5 mg/L ammonia (Fig.5A), while those of *IPR* were inversely correlated with ammonia concentrations (Fig.5B). In contrast, the mRNA levels of the remaining candidate genes elevated in response to ammonia. *PLC* expression exhibited a notable direct proportionality with ammonia levels, except for a slight decline at 1 mg/L (F [4, 30]=63.915, P=0; Fig.5C). The *PMCA*, *ptMCU*, and *SERCA* mRNA contents reached a maximum at 15 mg/L ammonia, with marked variations between treatments (F [4, 30]=417.898, 1939.207, and 289.865, P=0; Figs.5D, F, and G). Moreover, the ELISA

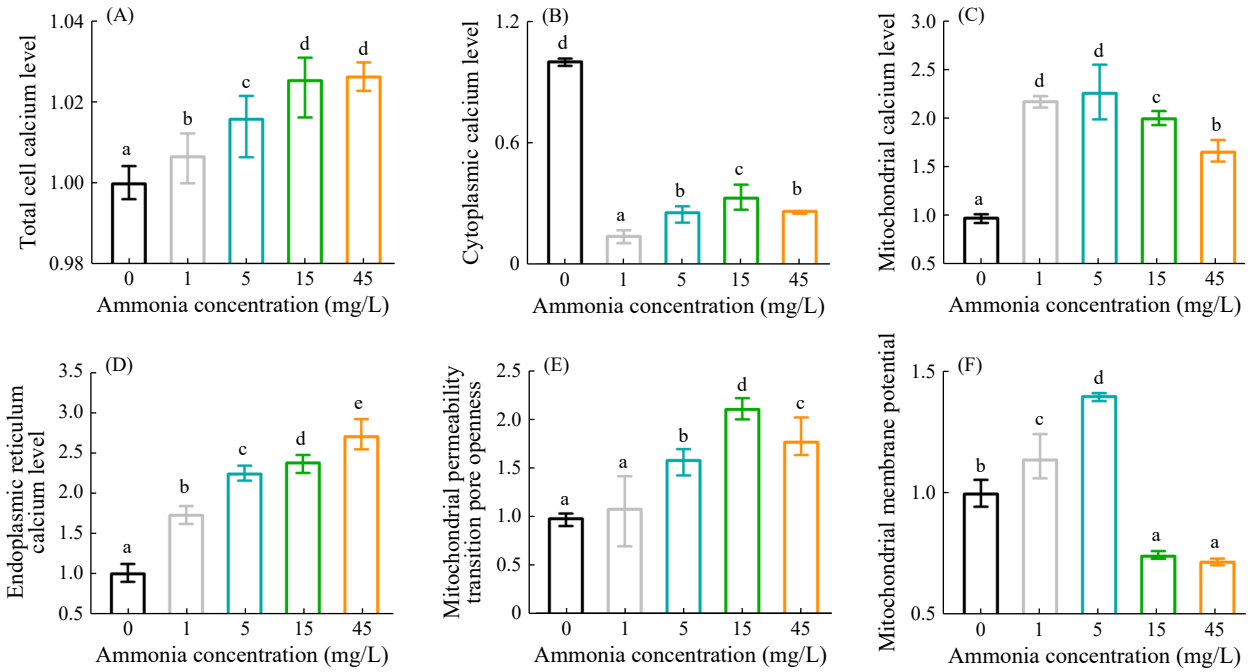

Fig.3 Dose-dependent effect of ammonia on Ca^{2+} homeostasis in hemocytes. (A), total Ca^{2+} level in hemocytes; (B), cytoplasmic Ca^{2+} level; (C), mitochondrial Ca^{2+} level; (D), endoplasmic reticulum Ca^{2+} level; (E), opening of mPTP; (F), ΔΨm. All data were expressed as a fold change compared to the control levels (exposure to 0 mg/L ammonia).

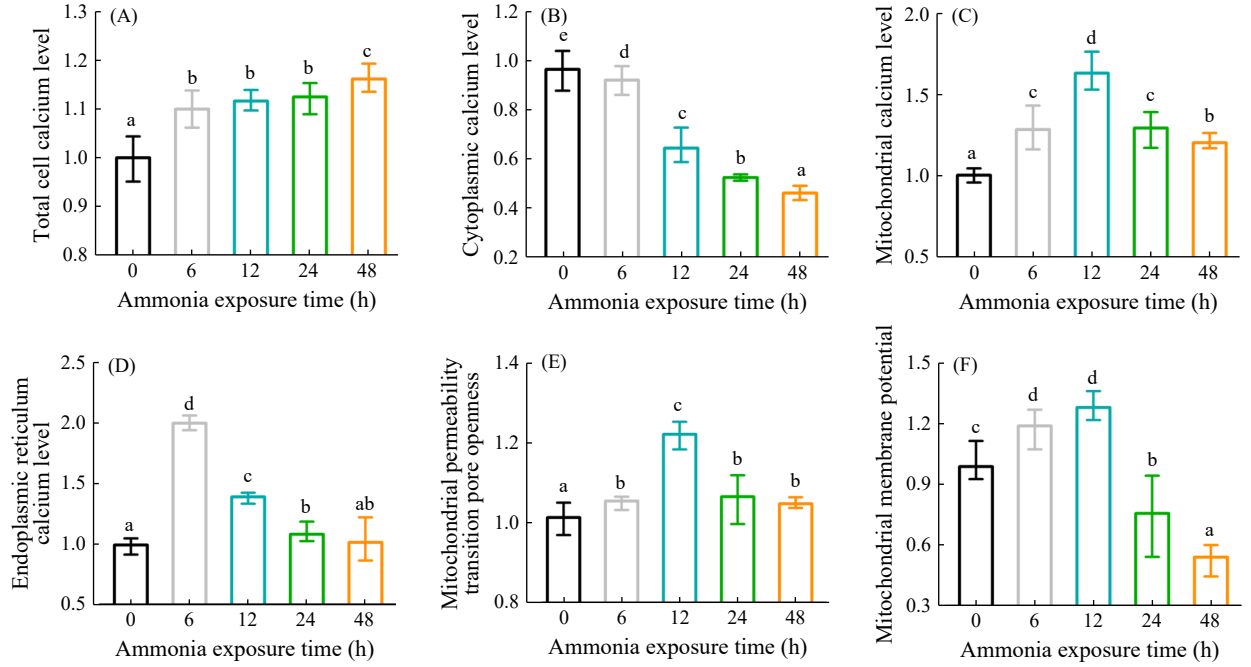

Fig.4 Temporal effects of ammonia on hemocyte Ca^{2+} levels. (A), total Ca^{2+} level in the hemocytes; (B), cytoplasmic Ca^{2+} level; (C), mitochondrial Ca^{2+} level; (D), endoplasmic reticulum Ca^{2+} level; (E), opening of the mPTP; (F), ΔΨm. All data are expressed as the fold change compared to the control level (at 0 h, *i.e.*, before ammonia exposure).

results indicated that ammonia at >5 mg/L also elevated the ptMCU protein levels (Fig.5E).

A notable decline in *LETM* expression was detected within 12 h of ammonia exposure, although an evident increase was detected at 48 h (F [4, 30]=259.364, P=0; Fig.6A). *IPR* expression was inversely correlated with the duration of ammonia-induced stress (F [4, 30]=135.511, P=0; Fig.6B). Conversely, elevated expression of other candidate genes was recorded, reaching a zenith at 24 or 48 h (F [4, 30]=297.475, 669.065, and 997.500, P=0; Figs.6C, D, and F]. However, *PMCA* was inhibited at 48 h (F [4, 30]=145.161, P=0; Fig.6G). A considerable increase in ptMCU protein levels was observed at 12 h of ammonia exposure (F [4, 30]=100.929, P=0; Fig.6A).

3.5 Ammonia Inhibited Mitochondrial Energy Production

In the dose experiment, the hemocyte ATP level was

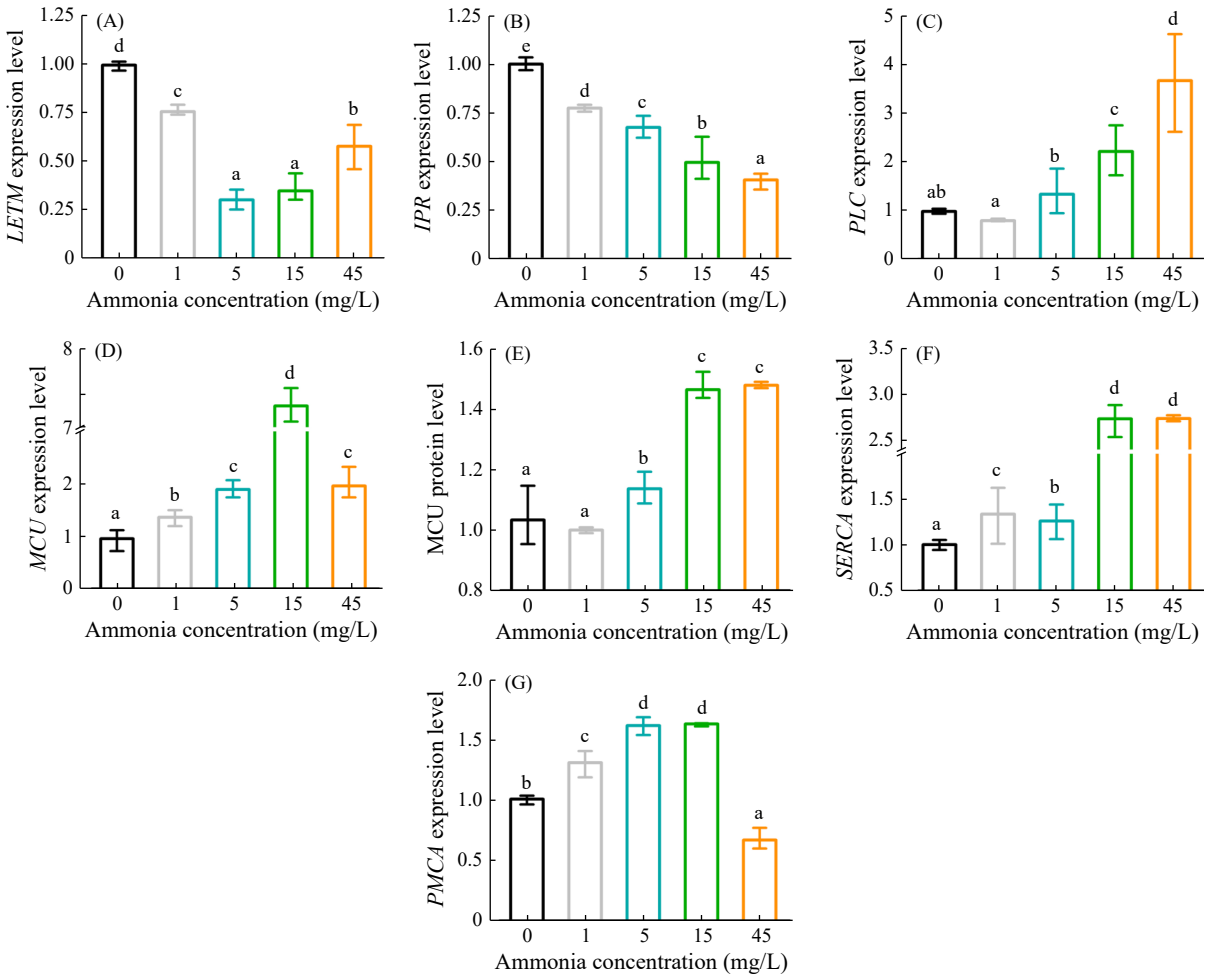

Fig.5 Dose-dependent effects of ammonia on the mRNA levels of Ca^{2+}-related genes in hemocytes.

remarkably elevated by ammonia at 1 mg/L, while it gradually declined with increasing ammonia levels ranging from 5 to 45 mg/L (F [4, 30]=69.582, P=0; Fig.7A). The ATP levels also folowed a comparable fluctuating pattern exhibiting an elevation at the 6 h mark post-ammonia exposure, followed by a reduction (F [4, 30]=99.664, P=0; Fig.7B).

3.6 MCU Inhibition Improved Mitochondrial Ca^{2+} Homeostasis

A notable alleviation in ammonia-induced mitochondrial damage following MCU blocking with RR was detected (Fig.8). In parallel with MCU inhibition (F [4, 30]= 19.403 and 10.284, P=0.001; Figs.8A and B), a reduction in $[Ca^{2+}]_m$ (F [4, 30]=84.397, P=0; Fig.8C) and mPTP opening (F [4, 30]=31.182, P=0; Fig.8D), along with an increase in cytosol $[Ca^{2+}]$ (F [4, 30]=169.826, P=0; Fig.8E), was observed in the RR group when compared to the ammonia exposure group. However, the loss in ΔΨm was exacerbated by RR treatment (F [4, 30]=82.938, P=0; Fig.8F). RR did not significantly impact $[Ca^{2+}]_{ER}$ (F [4, 30] =141.145, P=0; Fig.7B).

3.7 MCU Inhibition Improved Cell Health

Pearson correlation analysis (Figs.9A, B) revealed a positive relationship between ptMCU expression, $[Ca^{2+}]_m$, and ammonia-induced alterations in ROS levels, apoptosis, and ACF recorded in our previous study (Lu *et al.*, 2025). Subsequently, we investigated whether RR treatment could restore normal cell functioning. In comparison with the control group, ammonia exposure remarkably increased ROS accumulation, ratio of autophagic cells, and hemocyte apoptosis (F [2, 18]=44.224, 379.229, 95.403, and 191.853, P=0; Figs.9C–F). All these changes were significantly suppressed in the RR group, with the lysosomal fluorescence intensity decreasing to a level lower than that of the control (P=0). Based on these findings, a potential mechanism underlying hemocyte damage induced by ammonia *via* MCU was proposed (Fig.9G).

4 Discussion

High ammonia levels are a threat to animal health. Our study showed that ammonia-induced stress induced an aberrant regulation of MCU in the hemocytes of the crab *P. trituberculatus*. This alteration results in compromised hemocytic mitochondrial Ca^{2+} homeostasis, which is implicated in mitochondrial damage and subsequent apoptosis. These findings verified that MCU inhibition can be employed as an alternative method to ameliorate mito-

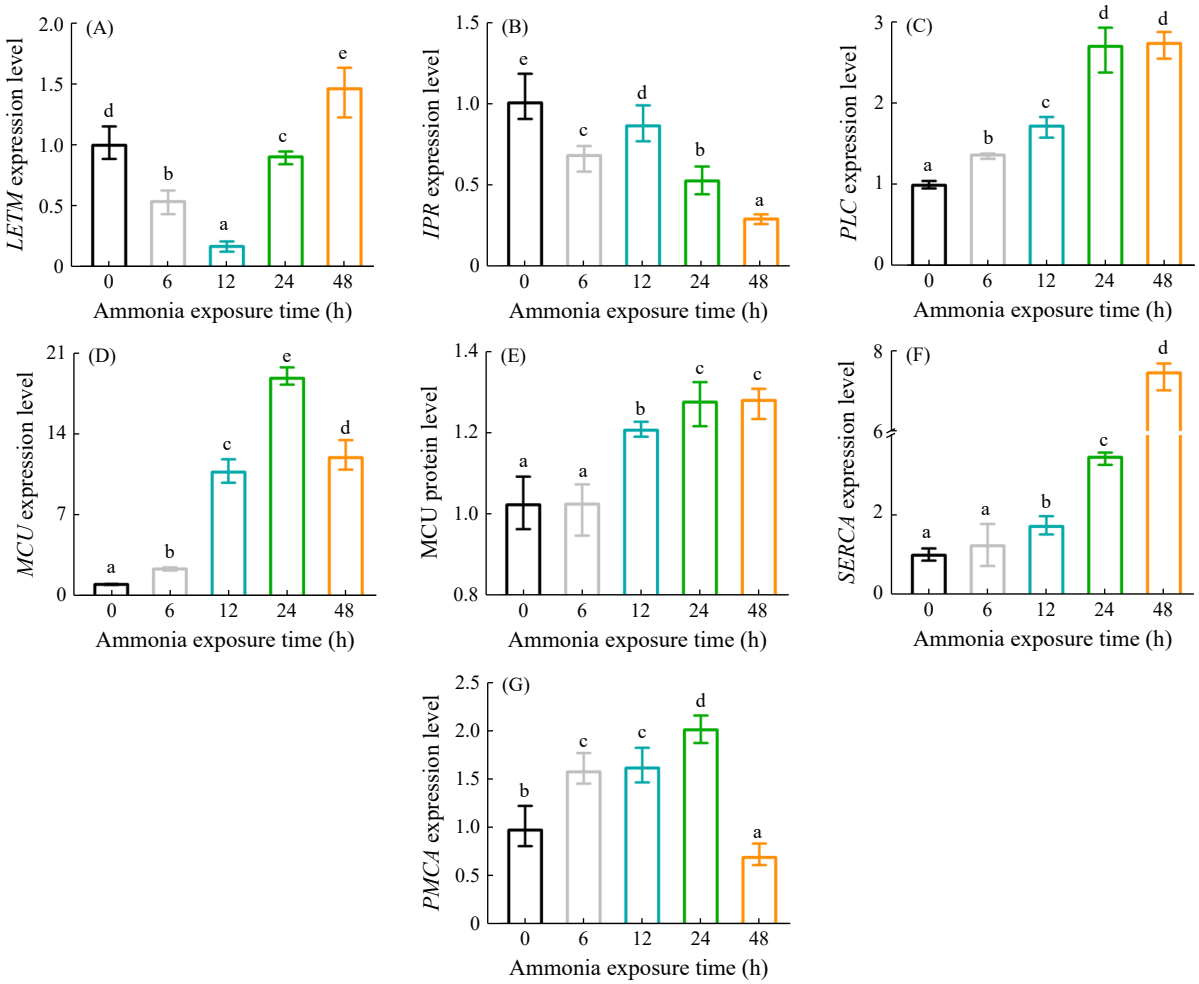

Fig.6 Temporal effects of ammonia on the mRNA levels of Ca^{2+}-related genes in hemocytes.

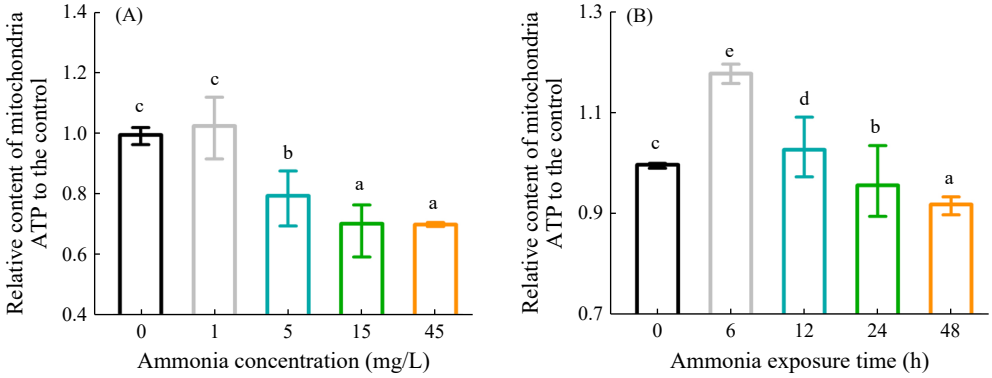

Fig.7 Dose-dependent (A) or temporal (B) effects of ammonia-induced stress on the ATP levels of hemocytes.

chondrial dyshomeostasis and consequently improve hemocyte health in natural or aquaculture systems.

Ca^{2+}-based signaling is vital for cell functions. The present study demonstrates that ammonia exposure enhanced the influx of Ca^{2+} from the extracellular space, as indicated by an elevated $[Ca^{2+}]_t$ in the hemocytes. Notably, a simultaneous increase in $[Ca^{2+}]_C$ was not identified; instead, demonstrating an opposing trend. Such observations may be partly ascribed to the augmented extrusion of Ca^{2+} from the cytosol to the extracellular space *via* the PMCA. PMCA is expressed ubiquitously in plasma membranes and constitutes a principal Ca^{2+} efflux pathway in non-excitable cells (Bruce, 2018; Patergnani *et al.*, 2020). In aquatic animals, PMCA can be stimulated by stimuli such as cold challenge (Han *et al.*, 2018) and bacterial infection (Fu *et al.*, 2019). Such a view is also corroborated by our finding that PMCA expression was upregulated in crab hemocytes to facilitate Ca^{2+} extrusion from the cells under HAE.

In fact, Ca^{2+} uptake by cell organelles contributes significantly to a reduction in the hemocyte $[Ca^{2+}]_C$. The mitochondria and ER serve as primary Ca^{2+} stores within cells, dynamically regulating $[Ca^{2+}]_t$ through coordinated mechanisms involving ATP-driven pumps. These include

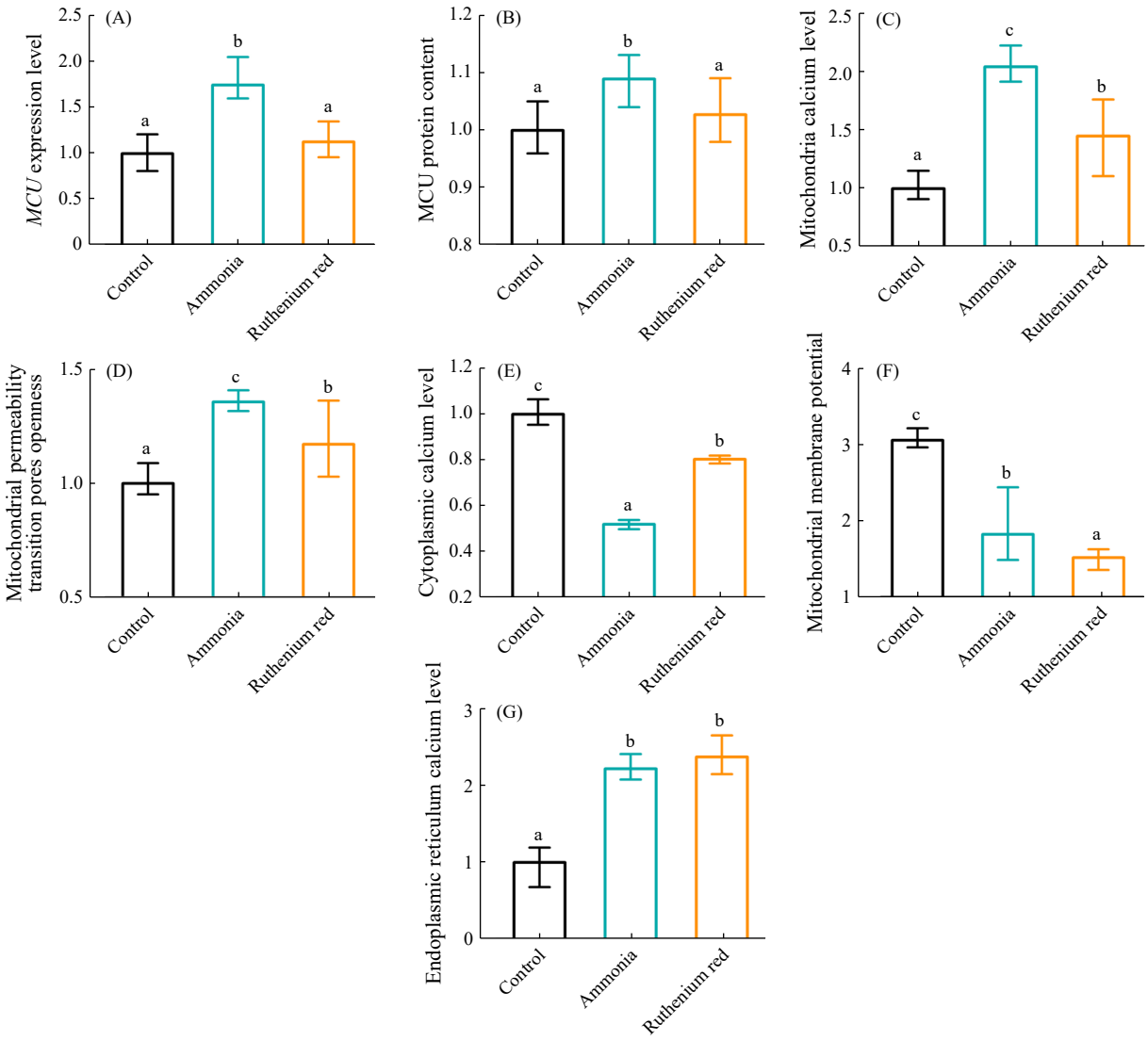

Fig.8 MCU inhibition with RR improved mitochondrial Ca^{2+} homeostasis. (A), mRNA levels of *MCU*; (B), protein levels of MCU; (C), mitochondrial Ca^{2+} level; (D), opening of the mPTP; (E), cytoplasmic Ca^{2+} level; (F), $\Delta\Psi m$; (G), the endoplasmic reticulum Ca^{2+} level.

the SERCA pump, which transports Ca^{2+} into the ER; the IP3R, which mediates the exchange of Ca^{2+} between the ER and mitochondria; the MCU and LETM1, a reversible IMM Ca^{2+}/H^{+} antiporter functioning in $[Ca^{2+}]_m$ efflux and uptake (Marchi *et al*., 2018; Garbincius and Elrod, 2022; Matuz-Mares *et al*., 2022; de Ridder *et al*., 2023). Previous studies on aquatic animals have indicated a Ca^{2+} overload in the mitochondria or ER in the presence of diverse contaminants (Diao *et al*., 2023; Miao *et al*., 2023; Liu *et al*., 2025). In *P. trituberculatus* exposed to ammonia, we observed a simultaneous alteration in the $[Ca^{2+}]_t$ and organelle-specific Ca^{2+} levels. The upregulation of *SERCA* and *MCU* suggests that HAE promotes Ca^{2+} influx, elevating cellular Ca^{2+} pools, a phenomenon also reported in *P. vannamei* exposed to ammonia at 0–11.3 mg/L, thereby inducing stress (Li *et al*., 2024). The consequent organelle-specific Ca^{2+} overload can also be attributed to the reduced efflux of Ca^{2+} into the cytosol, as suggested by a downregulation of *LETM1* and *IP$_3$R*. The decreased *IP$_3$R* expression indicates that HAE-induced $[Ca^{2+}]_m$ overload in these cells may be independent of ER–mitochondria Ca^{2+} transfer. This observation contradicts previous findings, where pollutants promoted the IP3R-mediated ER–mitochondria Ca^{2+} transfer in carps (*Cyprinus carpio*) (Liu *et al*., 2025) and *P. vannamei* (Li *et al*., 2024). These discrepancies highlight the diverse Ca^{2+} regulatory pathways across aquatic species.

The fluctuation in $[Ca^{2+}]_t$ is of great consequence to the overall health of the cell. In aquatic organisms, exposure to pollutants or pathogens can induce mitochondrial Ca^{2+} overload, serving as a stimulus that triggers programmed cell death, including apoptosis and necroptosis (Kumar *et al*., 2022; Diao *et al*., 2023; Miao *et al*., 2023; Liu *et al*., 2025). As the cell energy hub, mitochondria are highly sensitive to alterations in Ca^{2+}-based signaling. While moderate elevations in $[Ca^{2+}]_m$ can support mitochondrial metabolic activity and ATP production, excessive accumulation disrupts these processes, impairing oxidative phosphorylation, inducing mitochondrial damage, and subsequently activating autophagy-associated mechanisms, ulti-

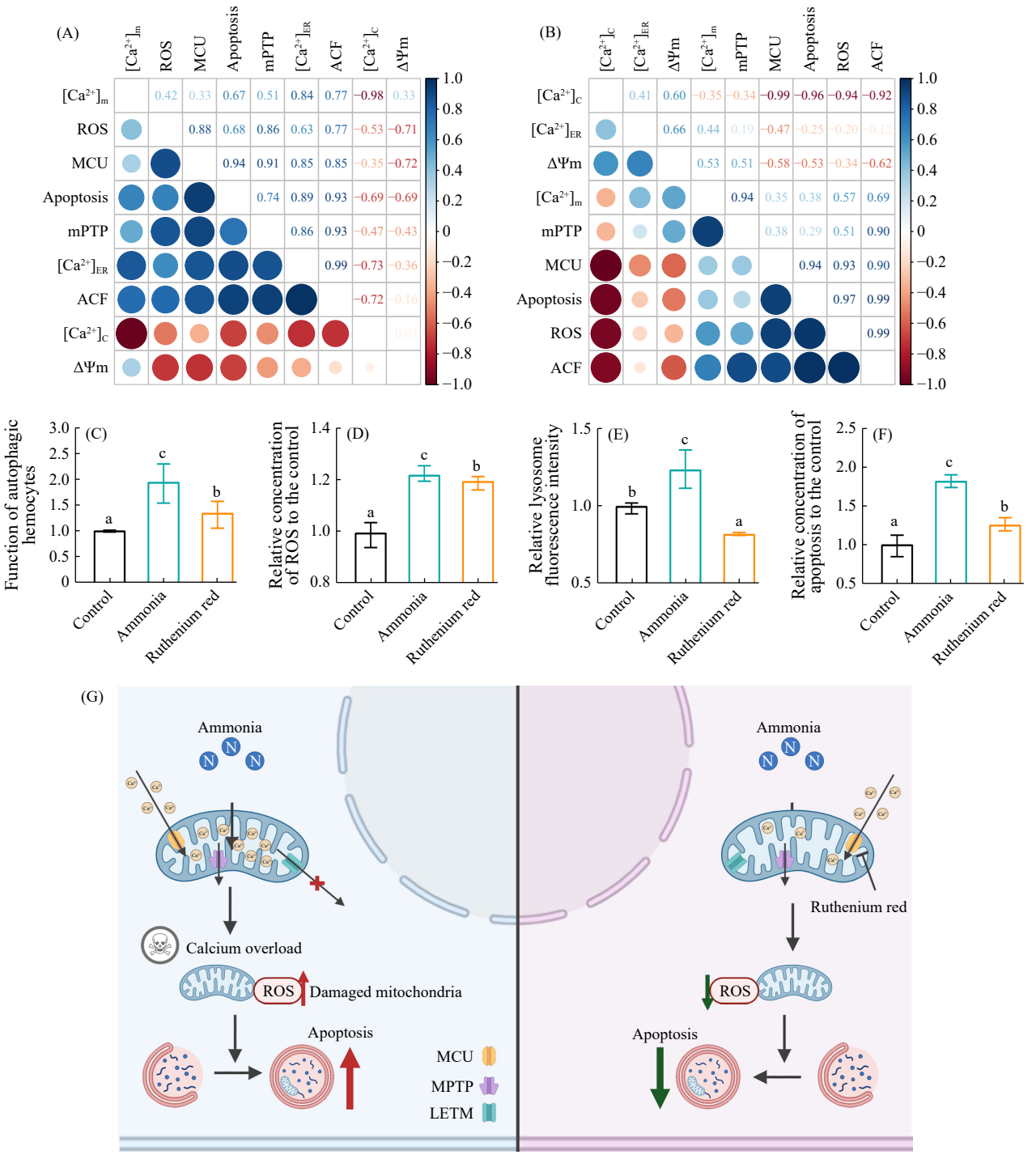

Fig.9 Relationship between MCU-mediated $[Ca^{2+}]_m$ homeostasis and ROS levels and autophagy in hemocytes. Pearson correlation analysis in terms of dose (A) and temporal (B) effects are shown. The blue and red colors indicate a positive and a negative correlation, respectively. The ROS levels, apoptosis, and autophagic cell fraction (ACF) were determined under the same stress conditions applied in our previous study. (C)–(F) The RR-induced changes in autophagy, ROS levels, lysosomal activity, and apoptosis, respectively, relative to the control level. (G) The postulated mechanism by which ammonia damaged hemocytes *via* the MCU. Briefly, the loss of MCU-mediated Ca^{2+} homeostasis triggered the opening of the mPTP and disrupted the membrane potential and, thereby, ETC function. This effect enhanced electron leakage and ROS production, which, in turn, elevated apoptosis. However, this phenomenon was mitigated by RR treatment.

mately resulting in apoptosis (Hou *et al.*, 2024). In the present study, a substantial reduction was observed in ATP levels and ΔΨm in crab hemocytes subjected to ammonia-induced stress. Furthermore, our previous work revealed that HAEs significantly elevated ROS accumulation, autophagic cell ratio, and apoptosis rates (Lu *et al.*, 2025), which positively correlated with MCU expression levels and $[Ca^{2+}]_m$. These observations collectively suggest that HAE can induce mitochondrial dysfunction in crab hemocytes by disrupting the MCU-mediated regulation of mitochondrial Ca^{2+} homeostasis.

Mitochondrial membrane permeability is essential in

maintaining cell health. In mammals, mitochondrial membrane permeabilization, often resulting from $[Ca^{2+}]_m$ overload, initiates a cascade of events, including cytochrome *c* release leading to cell death (Orrenius *et al*., 2015; Hou *et al*., 2024). However, the occurrence of a transition in mitochondrial membrane permeability induced by Ca^{2+} in crustaceans remains ambiguous. Our findings provide compelling evidence that ammonia-induced mPTP opening in *P. trituberculatus* hemocytes is closely linked to $[Ca^{2+}]_m$ and can be effectively mitigated by reducing $[Ca^{2+}]_m$ *via* MCU inhibition. Furthermore, mPTP opening may also occur in response to reductions in ΔΨm (Han *et al*., 2023) or excessive ROS accumulation (Díaz-Resendiz *et al*., 2020). In the present study, ammonia exposure elevated mPTP opening, accompanied by $[Ca^{2+}]_m$ overload, ATP depletion, and oxidative stress driven by ROS accumulation. It is thus postulated that HAEs may precipitate mitochondrial dysfunction in crab hemocytes through mechanisms involving $[Ca^{2+}]_m$ dysregulation and ROS-induced damage, ultimately leading to mPTP opening and a compromise in normal cell functioning.

These findings support the hypothesis that targeting MCU may improve hemocyte functionality to better modulate immune regulation in crustaceans. To validate the hypothesis that MCU-mediated Ca^{2+} homeostasis is essential for maintaining mitochondrial and hemocyte health, crabs were administered with RR, an MCU antagonist utilized in previous studies on *P. vannamei* (Rodriguez-Armenta *et al*., 2021). The findings demonstrate that MCU inhibition exerts a remarkable protective effect on mitochondria, characterized by a reduced $[Ca^{2+}]_m$ overload, ROS accumulation, and mPTP opening. Autophagy is an evolutionarily conserved process whereby dysfunctional proteins and organelles are degraded or recycled (Mizushima, 2007). Our previous findings (Lu *et al*., 2025) indicate that HAEs impair the anti-apoptotic role of autophagy in the hemocytes of *P. trituberculatus*. However, this detrimental effect could be mitigated by MCU inhibition conducted in the present study, as evidenced by a reduction in apoptosis and autophagic cell ratio. Interestingly, no induction of lysosomal activity, a key player in autophagy, was observed. Therefore, it is proposed that MCU suppression may prove beneficial in enhancing the healthy functioning of crab hemocytes, potentially through a reduction in the intracellular degradation load rather than an enhancement of the autophagy-mediated degradation.

Our findings highlight the potential of MCU inhibition as a strategic approach in aquatic or natural systems to mitigate ammonia-induced damage to hemocytes, which may contribute to the maintenance of vital functions such as immune regulation. However, the mechanisms underlying such an effect on hemocyte functions remain to be fully elucidated. Furthermore, the results suggest that ammonia-induced $[Ca^{2+}]_m$ overload in *P. trituberculatus* hemocytes appeared to be $[Ca^{2+}]_{ER}$-independent, as no significant change in $[Ca^{2+}]_{ER}$ was observed post-RR treatment.

5 Conclusions

Ca^{2+} acts as a critical regulator of numerous cell processes, and its homeostasis is maintained by proteins such as MCU. The present study demonstrates that Ca^{2+} overload is induced in the mitochondria and ER of hemocytes from *P. trituberculatus* upon ammonia exposure. It disrupts MCU-mediated $[Ca^{2+}]_m$ homeostasis, which can be mitigated by suppressing MCU, which reduces ROS-associated stress and mPTP opening. Consequently, a decline in the intracellular degradation burden, facilitated by the enhanced mitochondrial functionality, underpins the protective effects of MCU inhibition on crab hemocytes. These findings suggest that inhibiting MCU to improve the hemocyte status may hold potential value for maintaining hemocyte-associated functions, such as immune regulation, in crustaceans like *P. trituberculatus*. However, further studies are required to fully elucidate the underlying mechanisms and explore future applications of this approach.

Supplementary Materials

Supplementary materials are available in the online version of this article at https://doi.org/10.1007/s11802-026-6259-y.

Acknowledgements

This research was funded by the National Natural Science Foundation of China (Nos. 31972784 and 32373103), the Modern Agro-Industry Technology Research System in Shandong Province (No. SDAIT-13), the High-Level Talents Research Fund of Qingdao Agricultural University (No. 663/1119032), and the ‘First Class Fishery Discipline Programme’ in Shandong Province, China.

Author Contributions

Yingying Liu: investigation, validation, formal analysis, writing–original draft. Yueqi Zhang: investigation, validation, formal analysis. Jianwei Cao: investigation, formal analysis. Cunyan Zhao: investigation. Wenqi Wang: investigation. Fang Wang: investigation, funding, writing–review and editing. Yanting Cui: investigation, writing–review and editing. Yunliang Lu: conceptualization, investigation, formal analysis, resources, funding, writing–review and editing.

Data Availability

All data in the present study are presented in this article and supplementary files.

Declarations

Ethics Approval and Consent to Participate

As *P. trituberculatus* is a non-protected crustacean spe-

cies, no special authorization was required for this study.

Consent for Publication

Informed consent for publication was obtained from all participants.

Conflict of Interests

All authors declare that they have no conflict of interest.

References

Angelova, P. R., and Abramov, A. Y., 2024. Interplay of mitochondrial calcium signalling and reactive oxygen species production in the brain. *Biochemical Society Transactions*, **52**: 1939–1946.

Antonucci, S., Di Lisa, F., and Kaludercic, N., 2021. Mitochondrial reactive oxygen species in physiology and disease. *Cell Calcium*, **94**: 102344.

Bruce, J. I. E., 2018. Metabolic regulation of the PMCA: Role in cell death and survival. *Cell Calcium*, **69**: 28–36.

Chen, I. T., Aoki, T., Huang, Y. T., Hirono, I., Chen, T. C., Huang, J. Y., *et al*., 2011. White spot syndrome virus induces metabolic changes resembling the Warburg effect in shrimp hemocytes in the early stage of infection. *Journal of Virology*, **85**: 12919–12928.

Chen, J., Liu, P., Lin, Y., and Lee, C., 1988. Super intensive culture of red-tailed shrimp *Penaeus penicillatus*. *Journal of the World Aquaculture Society*, **19**: 127–131.

De Ridder, I., Kerkhofs, M., Lemos, F. O., Loncke, J., Bultynck, G., and Parys, J. B., 2023. The ER-mitochondria interface, where Ca^{2+} and cell death meet. *Cell Calcium*, **112**: 102743.

Diao, L., Ding, M., Sun, H., Xu, Y., Yin, R., and Chen, H., 2023. Micro-algal astaxanthin ameliorates polystyrene microplastics-triggered necroptosis and inflammation by mediating mitochondrial Ca^{2+} homeostasis in carp's head kidney lymphocytes (*Cyprinus carpio* L.). *Fish and Shellfish Immunology*, **143**: 109205.

Díaz Resendiz, K. J. G., Bernal Ortega, J. A., Covantes Rosales, C. E., Ortiz Lazareno, P. C., Toledo Ibarra, G. A., Ventura Ramon, G. H., *et al*., 2020. *In-vitro* effect of diazoxon, a metabolite of diazinon, on proliferation, signal transduction, and death induction in mononuclear cells of Nile tilapia fish (*Oreochromis niloticus*). *Fish and Shellfish Immunology*, **105**: 8–15.

Feissner, R. F., Skalska, J., Gaum, W. E., and Sheu, S. S., 2009. Crosstalk signaling between mitochondrial Ca^{2+} and ROS. *Frontiers in Bioscience–Landmark*, **14**: 1197–1218.

Fu, S., Ding, M., Liang, Q., Yang, Y., Chen, M., Wei, X., *et al*., 2019. The key differentially expressed genes and proteins related to immune response in the spleen of pufferfish (*Takifugu obscurus*) infected by *Aeromonas hydrophila*. *Fish and Shellfish Immunology*, **91**: 1–11.

Garbincius, J. F., and Elrod, J. W., 2022. Mitochondrial calcium exchange in physiology and disease. *Physiological Reviews*, **102**: 893–992.

Han, T. Y., Wu, C. Y., Tsai, H. C., Cheng, Y. P., Chen, W. F., Lin, T. C., *et al*., 2018. Comparison of calcium balancing strategies during hypothermic acclimation of tilapia (*Oreochromis mossambicus*) and goldfish (*Carassius auratus*). *Frontiers in Physiology*, **9**: 1224.

Han, Y., Zhang, Q., Chen, L., Zhao, J., and Yang, D., 2023. *In vitro* study of deltamethrin-induced extracellular traps in hemocytes of *Ruditapes philippinarum*. *Ecotoxicology and Environmental Safety*, **256**: 114909.

Holman, J. D., and Hand, S. C., 2009. Metabolic depression is delayed and mitochondrial impairment averted during prolonged anoxia in the ghost shrimp, *Lepidophthalmus louisianensis* (Schmitt, 1935). *Journal of Experimental Marine Biology and Ecology*, **376**: 85–93.

Hou, M., Zhang, Z., Fan, Z., Huang, L., and Wang, L., 2024. The mechanisms of Ca^{2+} regulating autophagy and its research progress in neurodegenerative diseases: A review. *Medicine*, **103**: e39405.

Huang, Y., and Ren, Q., 2020. Research progress in innate immunity of freshwater crustaceans. *Developmental and Comparative Immunology*, **104**: 103569.

Jomova, K., Raptova, R., Alomar, S. Y., Alwasel, S. H., Nepovimova, E., Kuca, K., *et al*., 2023. Reactive oxygen species, toxicity, oxidative stress, and antioxidants: Chronic diseases and aging. *Archives of Toxicology*, **97**: 2499–2574.

Konrad, C., Kiss, G., Torocsik, B., Adam-Vizi, V., and Chinopoulos, C., 2012. Absence of Ca^{2+}-induced mitochondrial permeability transition but presence of bongkrekate-sensitive nucleotide exchange in *C. crangon* and *P. serratus*. *PLoS One*, **7**: e39839.

Kumar, M., Sharma, S., Haque, M., Kumar, J., Hathi, U. P. S., and Mazumder, S., 2022. TLR22-Induced pro-apoptotic mtROS abets UPRmt-mediated mitochondrial fission in *Aeromonas hydrophila*-infected headkidney macrophages of *Clarias gariepinus*. *Frontiers in Immunology*, **13**: 931021.

Li, H., Li, Q., Wang, S., He, J., and Li, C., 2023a. Ammonia nitrogen stress increases susceptibility to bacterial infection via blocking IL-1R–Relish axis mediated antimicrobial peptides expression in shrimp. *Aquaculture*, **563**: 738934.

Li, W., Wang, Y., Li, C., Wang, F., and Shan, H., 2024. Responses and correlation among ER stress, Ca^{2+} homeostasis, and fatty acid metabolism in *Penaeus vannamei* under ammonia stress. *Aquatic Toxicology*, **267**: 106837.

Li, Y., Tong, R., Li, Z., Zhang, X., Pan, L., Li, Y., *et al*., 2023b. Toxicological mechanism of ammonia-N on haematopoiesis and apoptosis of haemocytes in *Litopenaeus vannamei*. *Science of the Total Environment*, **879**: 163039.

Liu, F., Li, S., Yu, Y., Sun, M., Xiang, J., and Li, F., 2020. Effects of ammonia stress on the hemocytes of the Pacific white shrimp *Litopenaeus vannamei*. *Chemosphere*, **239**: 124759.

Liu, F., Zhang, T., Ma, Y., Dong, J., and Sun, Y., 2025. Risk assessment of difenoconazole pollution in carp (*Cyprinus carpio*): Involvement of liver metabolism disorder and IP3R-Sig1R mediated mitochondrial Ca^{2+} overload. *Journal of Environmental Sciences*, **152**: 313–327.

Loncke, J., Kerkhofs, M., Kaasik, A., Bezprozvanny, I., and Bultynck, G., 2020. Recent advances in understanding IP_3R function with focus on ER-mitochondrial Ca^{2+} transfers. *Current Opinion in Physiology*, **17**: 80–88.

Lu, Y., Liu, Y., Cao, J., Zhang, Y., Zheng, Y., and Wang, F., 2025. Waterborne ammonia toxicity damages crustacean hemocytes via lysosome-dependent autophagy: A case study of swimming crabs *Portunus trituberculatus*. *Environmental Research*, **272**: 120985.

Lu, Y., Zhang, J., Cao, J., Liu, P., Li, J., and Meng, X., 2022. Long-term ammonia toxicity in the hepatopancreas of swimming crab *Portunus trituberculatus*: Cellular stress response and tissue damage. *Frontiers in Marine Science*, **8**: 757602.

Luciani, D. S., Gwiazda, K. S., Yang, T. L. B., Kalynyak, T. B., Bychkivska, Y., Frey, M. H. Z., *et al*., 2009. Roles of IP3R

and RyR Ca^{2+} channels in endoplasmic reticulum stress and β-cell death. *Diabetes*, **58**: 422–432.

Marchi, S., Patergnani, S., Missiroli, S., Morciano, G., Rimessi, A., Wieckowski, M. R., *et al*., 2018. Mitochondrial and endoplasmic reticulum calcium homeostasis and cell death. *Cell Calcium*, **69**: 62–72.

Martínez-Cruz, O., Chimeo, C., Rodríguez-Armenta, C. M., and Muhlia-Almazan, A., 2017. Crustacean bioenergetics: Mitochondrial adaptive molecular responses to face environmental challenges. *Journal of Shellfish Research*, **36**: 771–786.

Matuz-Mares, D., González-Andrade, M., Araiza-Villanueva, M. G., Vilchis-Landeros, M. M., and Vázquez-Meza, H., 2022. Mitochondrial calcium: Effects of its imbalance in disease. *Antioxidants*, **11**: 801.

Menze, M. A., Hutchinson, K., Laborde, S. M., and Hand, S. C., 2005. Mitochondrial permeability transition in the crustacean *Artemia franciscana*: Absence of a calcium-regulated pore in the face of profound calcium storage. *American Journal of Physiology—Regulatory, Integrative and Comparative Physiology*, **289**: 68–76.

Miao, Z., Miao, Z., Feng, S., and Xu, S., 2023. Chlorpyrifos-mediated mitochondrial calcium overload induces EPC cell apoptosis via ROS/AMPK/ULK1. *Fish and Shellfish Immunology*, **141**: 109053.

Mizushima, N., 2007. Autophagy: Process and function. *Genes & Development*, **21**: 2861–2873.

Nemani, N., Shanmughapriya, S., and Madesh, M., 2018. Molecular regulation of MCU: Implications in physiology and disease. *Cell Calcium*, **74**: 86–93.

Orrenius, S., Gogvadze, V., and Zhivotovsky, B., 2015. Calcium and mitochondria in the regulation of cell death. *Biochemical and Biophysical Research Communications*, **460**: 72–81.

Parvathy, A. J., Das, B. C., Jifiriya, M. J., Varghese, T., Pillai, D., and Kumar, V. J. R., 2023. Ammonia induced toxicophysiological responses in fish and management interventions. *Reviews in Aquaculture*, **15**: 452–479.

Patergnani, S., Danese, A., Bouhamida, E., Aguiari, G., Previati, M., Pinton, P., *et al*., 2020. Various aspects of calcium signaling in the regulation of apoptosis, autophagy, cell proliferation, and cancer. *International Journal of Molecular Sciences*, **21**: 8323.

Patnaik, B. B., Baliarsingh, S., Sarkar, A., Hameed, A. S. S., Lee, Y. S., Jo, Y. H., *et al*., 2024. The role of pattern recognition receptors in crustacean innate immunity. *Reviews in Aquaculture*, **16**: 190–233.

Pinto, M. R., Lucena, M. N., Faleiros, R. O., Almeida, E. A., McNamara, J. C., and Leone, F. A., 2016. Effects of ammonia stress in the Amazon river shrimp *Macrobrachium amazonicum* (Decapoda, Palaemonidae). *Aquatic Toxicology*, **170**: 13–23.

Rodriguez-Armenta, C., Reyes-Zamora, O., De la Re-Vega, E., Sanchez-Paz, A., Mendoza-Cano, F., Mendez-Romero, O., *et al*., 2021. Adaptive mitochondrial response of the whiteleg shrimp *Litopenaeus vannamei* to environmental challenges and pathogens. *Journal of Comparative Physiology B—Biochemical Systems and Environmental Physiology*, **191**: 629–644.

Stefan, C. J., 2020. Endoplasmic reticulum–plasma membrane contacts: Principals of phosphoinositide and calcium signaling. *Current Opinion in Cell Biology*, **63**: 125–134.

Vassalle, M., and Lin, C. I., 2004. Calcium overload and cardiac function. *Journal of Biomedical Science*, **11**: 542–565.

Yuan, R., Hu, Z., Liu, J., and Zhang, J., 2018. Genetic parameters for growth-related traits and survival in Pacific white shrimp, *Litopenaeus vannamei* under conditions of high ammonian concentrations. *Turkish Journal of Fisheries and Aquatic Sciences*, **18**: 37–47.

Yue, F., Pan, L., Xie, P., Zheng, D., and Li, J., 2010. Immune responses and expression of immune-related genes in swimming crab *Portunus trituberculatus* exposed to elevated ambient ammonia-N stress. *Comparative Biochemistry and Physiology A—Molecular & Integrative Physiology*, **157**: 246–251.

Zhang, T. X., Li, M. R., Liu, C., Wang, S. P., and Yan, Z. G., 2023. A review of the toxic effects of ammonia on invertebrates in aquatic environments. *Environmental Pollution*, **336**: 122374.

Zhao, M., Yao, D., Li, S., Zhang, Y., and Aweya, J. J., 2020. Effects of ammonia on shrimp physiology and immunity: A review. *Reviews in Aquaculture*, **12**: 2194–2211.

(Edited by Qiu Yantao)